

## Automated Processing of Post-Mortem Cortex Images Reveals Physiological Changes Associated with Dementia Sub-types

D. J. Cornforth<sup>1</sup>, H. F. Jelinek<sup>1</sup>, M. C. Teich<sup>2</sup> and S. B. Lowen<sup>3</sup>

<sup>1</sup>Charles Sturt University, Albury, Australia

E-mail: {dcornforth, hjelinek}@csu.edu.au

<sup>2</sup>Boston University

Boston, Massachusetts 02215, USA

E-mail: teich@bu.edu

<sup>3</sup>Brain Imaging Center, McLean Hospital,

Belmont, Massachusetts 02478, USA

E-mail: lowen@mclean.org

### Abstract

*Automated classification is a well established technique for pattern recognition. In this work, the focus is upon testing for detectable differences between categories, rather than upon building a model for predicting category from new data. We applied image processing and pattern recognition techniques to determine whether there are differentiating features in the structure of blood vessels of the cortex when comparing dementia, its subtypes, and normal cortex. We derived measures from images of tissue using multi fractal analysis, which complements more conventional image analysis techniques. Although statistical methods found no evidence of differences between dementia subtypes, several machine learning methods were able to correctly classify many instances, leading us to conclude that detectable difference do exist. Further investigation along these lines may provide new understanding of the causes, pathology and treatment of these diseases. Our findings demonstrate the utility of multi-fractal analysis combined with machine learning techniques in dementia research.*

### 1. Introduction

The goal of this study is to investigate the efficacy of automated classification algorithms for differentiating between disease subtypes, using multi-fractal spectra, lacunarity and integrated density measures. This is a novel approach to the automated classification of dementia subtypes, as these measures have not been previously applied to this problem. Our results indicate that these measures may be of use as not only did they identify differences in blood vessel patterns associated with different cortical areas, but also reveal an anatomical basis for differences between disease subtypes. This suggests that multi-fractal analysis is a useful tool in neuropathology that can be applied to the study of other central nervous system diseases where blood vessels are implicated.

Automated classification is a common goal of machine learning, and is the task of assigning a class label to a set of measurements. This is achieved by determining some relationship between a set of measurements and a corresponding set of values on a nominal scale that represent category or class. The relationship is obtained by applying an algorithm to training samples that are 2-tuples  $\langle \mathbf{u}, z \rangle$ , consisting of an input vector  $\mathbf{u}$  and a class label  $z$ . The learned relationship can then be applied to instances of  $\mathbf{u}$  in order to discover the corresponding class label  $z$  [1]. A number of machine learning techniques including Genetic Algorithms [2], and Neural Networks [3] have been shown to be very effective for solving such problems.

Whilst automated classification is commonly employed in pattern recognition tasks, it can also be used to indicate that groups can be distinguished on the basis of a given set of measurements. If the measurements are sufficient to distinguish between classes, this should be revealed by the success of classifier algorithms in predicting the class correctly for the majority of data records. In this work, we compare standard statistical techniques and several machine learning algorithms. The data used for this comparison are based on image data obtained from patients with

Alzheimer's disease, with vascular dementia due to small vessel disease, and with no known pathology.

The remainder of this paper is organized as follows. Section 2 gives an overview of current knowledge regarding dementia and its effects upon the structure of blood vessels in the cortex. Section 3 describes the analysis and classification of complex objects. Section 4 describes the machine learning methods applied. Section 5 describes the methods used. Section 6 presents results, and section 7 concludes the paper.

## 2. Alzheimer's and Small Vessel Disease Dementia

Dementia is a clinical syndrome which results from degeneration of the brain. There are number of different subtypes of dementia of which Alzheimer's disease (AD) is the most common. Vascular dementia is the second most common cause of dementia, and includes subtypes due to large vessel disease (i.e. infarcts) and small vessel disease. The brain relies on a capillary network of vessels to bring oxygen and nutrient-bearing blood. The oxygen perfuses from the vessels to the brain cells and sub-optimal perfusion will interfere with cellular mechanisms. Changes to the microvascular system of the brain have been demonstrated in both AD and SVD dementia. However, there has been little quantitative investigation of the capillary network in patients with dementia [4]. One of the current research questions is whether there are differentiating features in the structure of blood vessels of the cortex when comparing dementia, its subtypes and normal cortex.

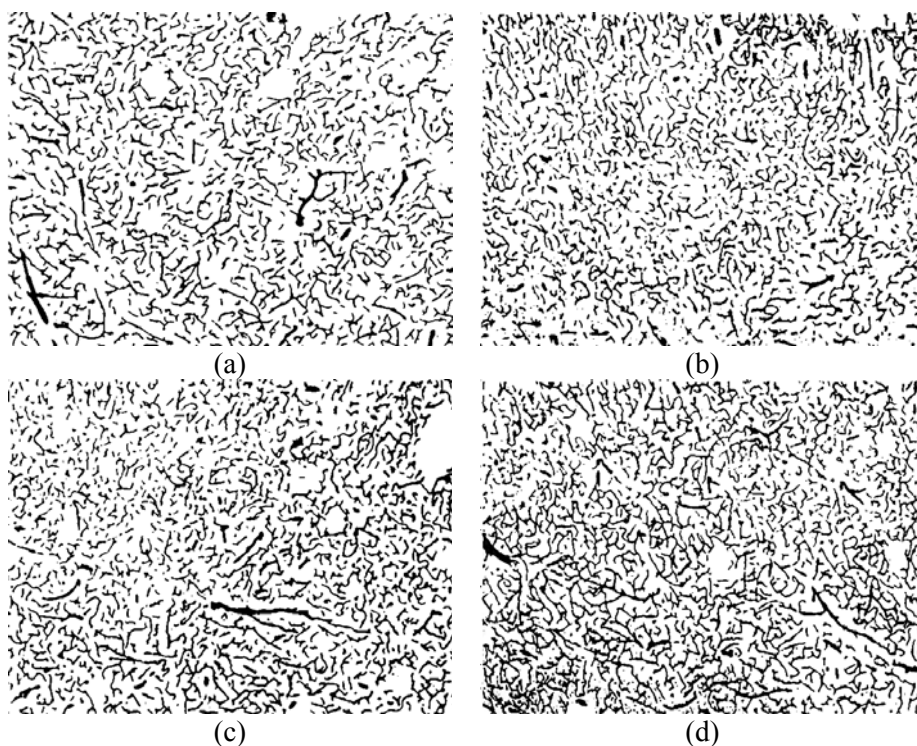


Fig. 1. Typical images of blood vessel structure obtained from the frontal lobe of patients with (a) Altzeimer's disease, (b) Small vessel disease, (c) both diseases, and (d) non-demented aged controls.

Figure 1 shows typical binary images of blood vessel structure obtained from the frontal cortex for patients with these four pathologies. The images in Figure 1 are of the frontal lobe showing in (a) AD, (b) SVD (c) AD-SVD and (d) non-demented control. Previous research has indicated that there may be a difference in vessel distribution or coverage between controls and dementia.

When viewing Figure 1 it becomes apparent that if such a difference exists, then it requires very sensitive pattern analysis, as traditional variables such as density and length of vessels cannot discriminate between these four cases.

### 3. Analysis of Complex Objects

Natural objects, including cells and tissues studied in pathology, have complex structural characteristics that are difficult to describe using Euclidean geometry. As an alternative, fractal analysis has found applications in the measurement of the space-filling properties of tumours, blood vessels, neurones and their support cells [5, 6, 7]. One of the tasks that pathologists routinely perform in diagnosis is the assessment of complexity of shape or texture of tissue such as muscle, bone or nervous tissue and microscopic images of individual cells, tumour growth and blood vessels [8, 9]. Some of these complex patterns can be approximated in terms of fractal structures and can be analysed using principles from global fractal or multi-fractal analysis [10].

Fractal analysis has been used extensively to characterise complex scaling phenomena in biological material [11]. Fractal analysis provides a quantitative parameter, generalised fractal dimension, for the extent to which an object fills space, and indicates whether scale-invariance is present [12]. However, the generalised dimension that is most often calculated does not always differentiate between structures due to their common scale-invariant properties [11, 6]. Multi-fractal analysis is a rather novel approach to analysing biological patterns [13, 14]. Multi-fractal analysis is based on the premise that structure is determined by many processes operating at different scales. The calculated multi-fractal spectrum reflects the diversity of the developmental or environmental influences contributing to the final complexity of the structures [15, 16]. Recently, multi-fractal analysis has been applied to biological tissues composed of complex structures and extended into the medical domain for analysing tumours and blood vessel complexity, especially for magnetic resonance images (MRI) [17, 18, 19].

The multi-fractal spectrum  $D(q)$  consists of many dimensions ranging from  $-\infty$  to  $+\infty$ . Of these only three are understood,  $D_0$ ,  $D_1$  and  $D_2$  [10].  $D_0$  is the *generalised* dimension or *Hausdorff* dimension,  $D_1$  is the *information* dimension and  $D_2$  is the *correlation* dimension. In practice one can use the box-counting method to obtain the multi-fractal spectrum by determining the probability  $P(m, \varepsilon)$  of finding  $m$  points in a box of size  $\varepsilon$ , estimated over different origins of the grid and for different box sizes [20]. For dimension  $q$  the corresponding scaling exponent  $D(q)$  can be obtained by

$$D(q) \approx \frac{1}{q-1} \left( \frac{\ln \sum_i p_i^q}{\ln \varepsilon} \right). \quad (1)$$

Although there are drawbacks to this method as discussed by Fernandez and co-workers [13], it is useful if only the positive spectrum is considered whilst the  $D(q)$  values are monotonically decreasing [10]. In particular, the case where  $q=1$  is normally solved by approaching 1 from both directions and taking the mean of these two values.

From the data a second parameter, the lacunarity, can also be determined [21]. Lacunarity is a multi-scale measure of texture describing the complex interactions of the shape and distribution of gaps within an image. Lacunarity was originally introduced to account for the finding that some images have the same fractal dimension value for visually different textures. It has so far

been mainly used for texture analysis other than biological features apart from the analysis of trabecular bone using CT images where it differentiated between images that differed only in the slice thickness [22]. Our analysis is the first to use lacunarity for pathological diagnosis. It is a useful parameter since many structures may have the same fractal dimension but differ in their lacunarity. Lacunarity can be defined as in equation 3, where  $\Lambda$  is the lacunarity and  $M(\varepsilon)$  are the statistical moments obtained from equation 4.

$$\Lambda(\varepsilon) = \frac{\langle M^2(\varepsilon) \rangle - \langle M(\varepsilon)^2 \rangle}{\langle M(\varepsilon)^2 \rangle} \quad (2)$$

$$M(\varepsilon) = \sum_{m=1}^N m^q P(m, \varepsilon) \quad (3)$$

#### 4. Machine Learning Methods

Machine learning is a powerful tool for classification type problems in pathology [23]. Up to now, very little use has been made of this tool in cellular and vascular pathology. Inductive decision tree analysis, logistic regression, back propagation neural networks and learning vector quantification have been some of the methods used to differentiate between malignant and normal cells [24, 25, 26]. Improved results have been reported for machine learning compared to linear and quadratic discriminant functions or logistic regression analysis [27, 28]. Cluster analysis has been reported in human pathology for identifying proliferative and angiogenic (blood vessel formation) activity [29, 30].

A number of automated classifier algorithms are available using the excellent Weka toolbox [31]. These are briefly discussed below and include the Decision Table, Nearest Neighbours, Decision Tree Induction, Kernel Density and Naïve Bayes algorithms. We also used an implementation of the CMAC neural network, which is not included in the Weka toolbox.

The *Decision Table* algorithm divides the dataset into cells, where each cell contains identical records. A record with unknown class is assigned the majority, or most frequent, class represented in the cell. The goal of training is to find a minimum set of attributes that are optimal in predicting the class [32].

The *Nearest Neighbours* algorithm [33] simply stores samples. When an example is presented to the classifier, it looks for the nearest match from the examples in the training set, and labels the unknown example with the same class. In practice the algorithm looks at the nearest  $k$  neighbours, where  $k$  is a parameter set by the user. We have used this algorithm with  $k=1$  and  $k=3$ .

The *Decision Tree Induction* algorithm [34] uses the C4.5 algorithm to form a tree by splitting each variable and measuring the information gain provided. The split with the most information gain is chosen as the first split, then the process is repeated until the information gain provided is below a threshold.

The *Kernel Density* algorithm [35] estimates a probability distribution of the data separately for each class. Each point is represented by a kernel function, and the kernels for all points in the class are summed to provide a composite function. An unknown point is evaluated by each

composite function separately, and the class function corresponding to the highest probability is chosen.

The *Naïve Bayes* algorithm [36] assumes that attributes are independent. From the correlation analysis above, we know this is untrue, but the algorithm performs surprisingly well. It estimates prior probabilities by calculating simple frequencies of the occurrence of each attribute value given each class, then returns a probability of each class, given an unclassified set of attributes.

The *Cerebellar Model Articulation Controller* (CMAC) [37] with the *Kernel Addition Training Algorithm* [38] divides the input space using multiple overlapping grids and builds a probability density function for each class. An unknown input then can be associated with an appropriate probability value for each class. The input is assigned to the class having the largest probability.

The *Default Classifier* is used as a “straw man” against which to assess the other algorithms. The idea is to assign the unknown record to the most frequently occurring class in the whole dataset, but this must take account of cross validation, which will be used to assess the other algorithms. Given a dataset containing  $s$  samples, selecting the most frequent class in the remaining  $n_s - 1$  samples will result in 0 correct guesses for datasets where the number of records in each class is similar. A better method is to select a record at random from the remaining  $s - 1$  samples, and choose the class of that record. If the dataset contains  $k$  classes, with the number of samples in each class given by  $\{n_1 \dots n_k\}$ , the expected number of correct guesses is given by equation 4. This value was calculated for each problem by manual inspection of the datasets, and is provided in table 2.

$$c = \frac{1}{s-1} \sum_{j=1}^k n_j - 1. \quad (4)$$

## 5. Methods

The microvascular network was visualised using appropriate methods described elsewhere [39]. Grey scale images of cortex were obtained using a Sony CCD video camera on an Olympus microscope attached to an IBM computer using Optimas software. Images (640x480 pixels) were optimised by obtaining 3 images of each region with fixed brightness, contrast and filter permutations and combining these images using the public domain software Object-Image (NIH) on a Macintosh computer. The resultant image was thresholded to provide a binary image. We obtained 50 images, comprising 18 from the parietal region (side of brain), 20 from the frontal region (front of brain) and 12 from the occipital region (rear of brain).

The multi-fractal spectrum was obtained using a macro based on the box-counting method, provided by NIH, in conjunction with a purpose written program. Our other measures were provided by NIH. Here mean density is the average grey value within the selection. This is the sum of the grey values of all the pixels in the selection divided by the number of pixels. Standard deviation of the grey values is our second variable. Integrated Density is the sum of the grey values in the selection, with background subtracted. This is calculated as

$$ID = \frac{(sum\_grey - background)}{N}. \quad (5)$$

Our program calculated the lacunarity from the box-counting analysis using

$$\Lambda(\varepsilon) = \frac{\text{Variance}}{(\text{mean})^2}. \quad (6)$$

The values obtained from the multi-fractal analysis were all highly correlated with each other; so one value was selected on the basis of minimum correlation with other measures. The correlation dimension  $D_2$  measure was selected, and this was used in the machine learning classification experiments. Images were also identified by the presentation or diagnosis, a nominal variable representing the class. This takes a value of AD for Alzheimer's disease, SVD for small vessel disease, AD-SVD for both, and CONTROL for normal (non-diseased tissue).

A fully crossed two fixed factor Analysis of Variance (ANOVA) was performed to test for differences in brain tissue using the measures of integrated density, correlation coefficient, and lacunarity between patients with and without small vessel disease, and with and without Alzheimer's disease. Separate analyses were performed for integrated density, correlation dimension, and lacunarity, using data from the frontal and parietal brain tissues. The amount of data available from the occipital region was smaller so precluded these data from the analysis. An F-test was used to test the null hypothesis that data were drawn from the same population, regardless of the diagnostic label.

We used the seven machine learning algorithms mentioned in the previous section, to classify records into four classes (AD or SVD or AD-SVD or CONTROL) and also to classify records into two classes (disease (AD, SVD, AD-SVD), or CONTROL). This was repeated for data from the three regions. The small amount of data from the Occipital region precluded investigation of the four class problem. The performance of the algorithms was tested using leave-one-out cross validation in order to avoid over fitting [40]. Accuracy was measured as the number of correctly predicted class labels. All classifier algorithms are deterministic, so the model produced should depend only upon the data set used. Nevertheless, we repeated each test 20 times to check that the implementation does not introduce any stochastic element.

## 6. Results

The multi-fractal spectrum is shown in Figure 2 for the ranges where  $D(q)$  is monotonically decreasing and the measure (dimensions) can be said to be multi-fractal when analysed using box-counting. A difference is apparent between frontal/parietal and occipital cortex for all  $D(q)$ . This suggests that the occipital lobe has a different small vessel structure irrespective of pathology or our sample cohort had occipital lobe atrophy. With respect to differentiating pathologies, AD-SVD has higher  $D(q)$  values compared to other pathologies and control in the frontal cortex. In the parietal cortex it is AD that has overall lower  $D(q)$  values compared to the other groups. In the parietal cortex the pathologies are more clearly differentiated for higher  $D(q)$  values, all being separated from the control MF spectrum except for AD-SVD. In the occipital cortex the  $D(q)$  spectrum has lower values and shows only a slight differentiation between AD (1 case only) compared to both control and AD-SVD spectra in  $D(q)$  values above 1.

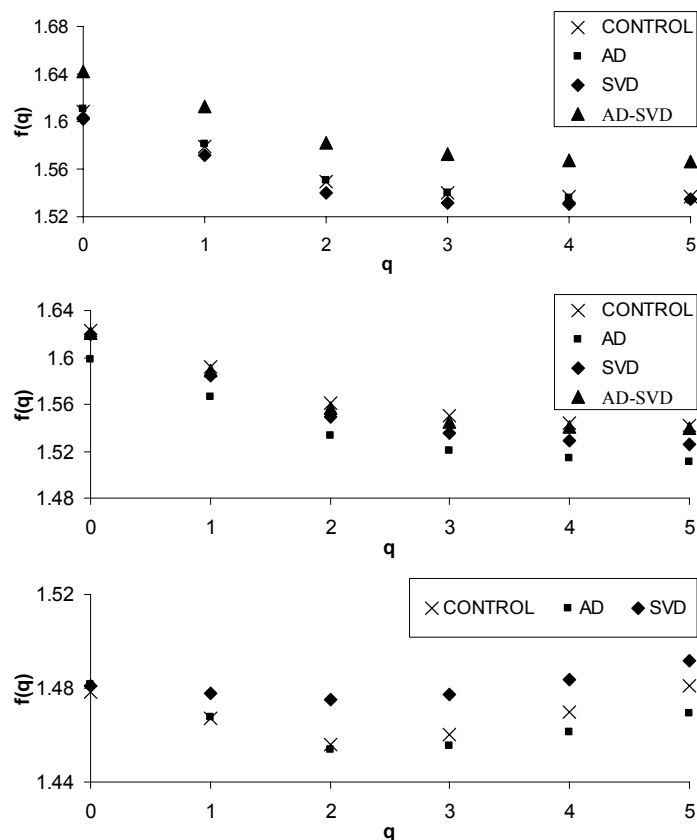


Fig. 2. Multi-fractal spectrum for frontal cortex (top), parietal cortex (middle), and occipital cortex (bottom).

When considering differences between the dementia sub-types, the control group had the smallest fractal dimension ( $D_2 = 1.519$ ) and SVD the largest ( $D_2 = 1.544$ ). AD had a  $D_2$  of 1.535 and AD-SVD a  $D_2$  of 1.531 reflecting differences in the aetiology of these dementia subtypes.

The values of lacunarity indicate that variability between gaps of vessel patterns were greater in the occipital lobe compared to the frontal and parietal lobe (0.58, 0.53, 0.52). For our control and pathology groups we found controls to have the largest lacunarity followed by AD-SVD, AD and SVD respectively (0.5409, 0.5343, 0.5306, 0.5278). In a relatively homogeneous image, as the lacunarity approaches 1, the variation in gap size distribution is minimal. This is reflected by the control group having the highest lacunarity index and suggesting an optimal blood vessel distribution throughout the cortex.

The results of the ANOVA test found no evidence (at the 95% CI level) that the presence of Alzheimer's disease or vascular disease influenced levels of integrated density, correlation dimension, or lacunarity in the frontal or parietal tissues of any of the patients (Table 1). However, these figures suggest that we might expect better results from the parietal region than from the frontal region, as the F values obtained are higher for the former.

Table 1. Results of ANOVA test for samples obtained from the Frontal and Parietal regions.

<b>Measurement</b>	<b>Frontal</b>			<b>Parietal</b>		
	<b>F value</b>	<b>df</b>	<b>P value</b>	<b>F value</b>	<b>df</b>	<b>P value</b>
integrated density	0.59	3,16	0.63	2.64	3,13	0.09
correlation dimension	0.88	3,16	0.47	1.76	3,13	0.20
lacunarity	0.74	3,16	0.54	0.9	3,13	0.47

Results of the machine learning experiment are summarised in table 2. Although all tests were repeated 20 times, no difference in accuracy was found for subsequent runs using the same data set. This confirms that the machine learning implementations do not introduce stochastic elements. The numbers shown in bold face are those results where the machine learning method achieved better accuracy than the default classifier, and imply some success in separating classes of dementia using the measurements described previously.

Columns 2 and 3 show the number of correctly classified records using data obtained from the Frontal region only. Column 2 shows the results of the four-class problem, while column 3 shows the results from the 2-class problem. Most of the algorithms, apart from the *CMAC*, performed badly on the Frontal 4-class problem. The *CMAC* is known to have a large number of model parameters, or weights [38], so the model produced is inherently less stiff than models produced by the other methods. Therefore over-fitting of the model cannot be ruled out. This is supported by the results from the *Nearest Neighbours* algorithm. Setting the number of neighbours to 3 ( $k=3$ ) would be expected to produce a stiffer model which here results in a useless model (accuracy = 0 out of 20), while a less stiff model ( $k=1$ ) results in a more accurate model (3 out of 20). We therefore doubt that there is sufficient information in the measurements used to reliably separate these classes. The results for the Frontal 2-class problem are much better, with five out of seven models produced achieving better accuracy than the default classifier, and three of these getting 14 correct out of 20. We conclude that there is probably sufficient information in the measurements used to reliably separate these classes.

Columns 4 and 5 show results for the four-class and two-class problem using data from the Parietal region. Column 4 shows results from the 4-class problem. Most of the machine learning algorithms did much better than the default classifier, apart from *Decision Table*, which appears to perform poorly on nearly every problem. Although 9 correct records out of 18 does not sound very successful, this compares favourably to the default classifier, which suggests that only 3.8 records could be correctly predicted using a random guess. Column 6 shows results from the 2-class problem. Here all of the machine learning algorithms performed better than the default classifier, with the best performance of 15 out of 18 records correctly identified, compared with 10.4 for a random guess. It appears that the data available from the Parietal region is sufficient to correctly classify disease types based on the measurements obtained. This implies that, in the Parietal region, the various disease subtypes are indeed associated with physical changes that are manifest in the structure of the microvascular system.

Column 6 shows results for the two-class problem from the Occipital region. All the algorithms apart from the *CMAC* performed very poorly on this problem. There is clearly insufficient evidence here for a link between disease subtype and the structure of the microvascular system.

Table 2. Results of the machine learning experiment.

Classifier	Frontal 4-class	Frontal Disease	Parieta l 4-class	Parieta l Disease	Occipita l Disease
Number of records	20	20	18	18	12
Default	4.4	11.2	3.8	10.4	5.5
CMAC	<b>6</b>	<b>14</b>	<b>9</b>	<b>13</b>	<b>7</b>
Decision Table	0	<b>14</b>	0	<b>12</b>	0
N.Neigh. $k=1$	3	10	4	<b>13</b>	3
N.Neigh. $k=3$	0	10	<b>9</b>	<b>15</b>	5
Decision Tree	2	<b>14</b>	<b>8</b>	<b>13</b>	0
Kernel Density	2	<b>13</b>	<b>9</b>	<b>14</b>	4
Naïve Bayes	2	<b>12</b>	<b>9</b>	<b>15</b>	5

Overall these results were better than would be expected from the results of the ANOVA tests, which show that such differences were not statistically significant. However, the ANOVA test makes the assumption of a Normal distribution and equal variances, and is robust only for large sample size. Furthermore, the ANOVA uses only one measurement in each test, whereas the machine learning methods are able to combine multiple measurements in one test, and fit complex discriminant functions to the resulting multidimensional space.

## 7. Conclusions

In this study, we have made use of measurements and techniques that have not previously been applied to the classification of dementia sub-types. Our results suggest that dementia subtypes can be distinguished from images of cortical tissue, as long as suitable measurements are used. Differences between dementia subtypes were most marked in data from the Parietal region. We conclude that there are differences between the structures of small blood vessels in subjects with dementia subtypes. This implies that physical changes underlying dementia are manifest by features in the microvascular system, and that these changes are detectable using analysis based on well-established techniques.

Multi-fractal spectra showed differences between images obtained from different locations, suggesting that it is possible to discriminate between these locations based on these measures alone. These spectra also showed some differences between disease subtypes and control for higher  $D(q)$  values. This suggests a complex interaction between parameters leading to the expression of a particular clinical subtype. Lower  $D_2$  values found for the occipital lobe confirm anatomical differences between the lobes rather than an age or disease affect. This needs to be considered in future research. The lowest value of lacunarity was found for SVD, which confirms blood vessel pathology as a causative factor in this dementia subtype.

Statistical methods using ANOVA found no evidence of difference between disease subtypes. However this technique relies on the assumption of a normal distribution, in contrast to the machine learning methods. A larger sample size may increase the power for the ANOVAs allowing a better chance of statistically detecting an effect. This is hampered by the scarcity of suitable images of diseased brain tissue. Sources of error that may have reduced the power of the ANOVA include the pixel resolution of the photographs as well as not including age as a variable. An improved statistical design may be to reduce between patient/brain variability by measuring each brain in both the parietal and frontal areas rather than the independent samples paradigm as performed in our study. One ANOVA could then partition out variability between different patients before testing for disease effects.

The machine learning techniques did provide evidence of a difference between dementia subtypes, and suggest that these pathologies may be associated with detectable changes in structure of small blood vessels in the cortex. The success of these methods appears to depend upon the area of the cortex studied, with samples from the Parietal region providing the most promising results. As with the ANOVA analysis, a larger sample size may also improve the machine learning outcomes.

We have addressed an important research question in the understanding of dementia. We have proposed suitable differentiating features based on images of the structure of blood vessels of the cortex. We have presented evidence for a difference between dementia, small vessel disease, and

normal cortex. This has implications for the understanding of this group of diseases, as well as for the analysis of cortical images in other contexts.

## References

- [1] T.G. Dietterich, and G. Bakiri, Solving Multiclass Learning Problems Via Error-Correcting Output Codes. *Journal of Artificial Intelligence Research*, Vol. 2, 263-286, 1995.
- [2] J. Holland, Adaptation in Natural and Artificial Systems: *An Introductory Analysis with Applications to Biology, Control, and Artificial Intelligence*, MIT Press, second edition, 1992.
- [3] R.O. Duda and P.E. Hart, *Pattern Classification and Scene Analysis*, John Wiley and sons, New York, 1973.
- [4] E. Englund, Neuropathology of white matter changes in Alzheimer's disease and vascular dementia, *Dementia & Geriatric Cognitive Disorders*, Vol. 9 (Suppl), No. 1, 6-12, July 1998.
- [5] S.S. Cross, Fractals in pathology, *Journal of Pathology*, Vol. 182, No. 1, 1-8, 1997.
- [6] E. Fernandez and H.F. Jelinek, Use of fractal theory in neuroscience: methods, advantages and potential problems, *Methods*, Vol. 24, No. 4, 309-321, 2001.
- [7] Z. Solty, M. Ziaja, R. Pawlinski, Z. Setkowicz, and K. Janeczko, Morphology of reactive microglia in the injured cerebral cortex. Fractal analysis and complementary quantitative methods, *J. Neurosci. Res.*, Vol. 63, 90-97, 2001.
- [8] G. Landini and J.G. Geake, Discrimination of complex histopathological tumour profiles by experienced and inexperienced observers, *J. Oral Pathology & Medicine*, Vol. 26, No. 10, 477-479, 1997.
- [9] E. Sabo, A. Boltenko, Y. Sova, A. Stein, S. Kleinhaus and M.B. Resnick, Microscopic analysis and significance of vascular architectural complexity in renal cell carcinoma, *Clinical Cancer Research*, Vol. 7, No. 3, 533-537, 2001.
- [10] J. Feder, *Fractals*, Plenum Press, N.Y., 1988.
- [11] T.G. Smith, W.B. Marks, G.D. Lange, W.H. Sheriff Jr, and E.A. Neale, A fractal analysis of cell images, *J. Neurosci. Meth.*, Vol. 27, 173-180, 1989.
- [12] H.F. Jelinek and I. Spence, Categorisation of physiologically and morphologically characterised non-alpha / non-beta cat retinal ganglion cells using fractal geometry, *Fractals*, Vol. 5, No. 4, 673-684, 1997.
- [13] Fernandez, E., Bolea, J.A., Ortega, G. and Louis, E. (1999) Are neurons multifractals? *J. Neurosci. Meth.* 89:151-157.
- [14] Smith, T.G. and Lange, G.D. (1998) Biological cellular morphometry-fractal dimensions, lacunarity and multifractals. In: *Fractals in Biology and Medicine*, Vol. 2. Eds Losa, G.A., Merlini, D., Nonnenmacher, T.F., Weibel, E.R. Birkhauser, Basel. 30-49.
- [15] Block, A., von Bloh, W. and Schnellhuber, H.J. (1990) Efficient box-counting determination of generalised fractal dimensions. *Phys. Rev. A*. 42(4):1869-1874.
- [16] Takayasu, H. (1990) *Fractals in the physical sciences*. Manchester University Press, Manchester.
- [17] Caligiuri, P., Giger, M.L. and Favus, M. Multifractal radiographic analysis of osteoporosis. *Med. Phys.* 21(4):503-508. 1994.
- [18] Heymans, O., Blacher, S. Brouers, F. and Pierard, G.E. Fractal quantification of the microvasculature heterogeneity in cutaneous melanoma. *Dermatology*. 198:212-217. 1999.
- [19] Takahashi, T., Murata, T., Omori, M., Kimura, T., Kado, H., Kosaka, H., Takahashi, K., Itoh, H. and Wada, Y. Quantitative evaluation of magnetic resonance imaging of deep white matter hyperintensity in geriatric patients by multifractal analysis. *Neuroscience Letters*. 314(3). November 16, 2001. 143-146.
- [20] Vicsek, T. (1992) *Fractal Growth Phenomena*. World Scientific, Singapore.
- [21] Landini, G.(1995) Applications of fractal geometry in pathology. In: *Fractal Geometry in Biological Systems: an analytical approach*. Eds Iannaccone, P.M. and Khokha, M. CRC Press, New York, 205-242.
- [22] Douherty, G. and Henebry, G.M. Fractal signature and lacunarity in the measurement of the texture of trabecular bone in clinical CT images. *Med. Eng. Physics*, 23:369-380. 2001.
- [23] Jelinek, H.F., Maddalena, D.J. and Spence, I. (1994) Application of artificial neural networks to

- cat retinal ganglion cell categorization. Proc. 5th Australian Conference on Neural Networks, pp:177-180.
- [24] Karakitsos, P., Stergiou, E.B., Pouliakis, A., Tzivras, M., Archimandritis, A., Liossi, A. and Kyrokou, K. Comparative study of artificial neural networks in the discrimination between benign from malignant gastric cells. *Analytical & Quantitative Cytology & Histology*. 19(2). 1997. 145-152.
- [25] Wolfberg, W., Street, W.N., Heisey, D.M. and Mangasarian, O.L. Computer-derived nuclear features distinguish malignant from benign breast cytology. *Human Pathology*. 26(7). 1995. 792-796.
- [26] Hurwitz, G.A. The predictive and explanatory power of inductive decision trees: A comparison with artificial neural network learning as applied to the noninvasive diagnosis of coronary artery disease. *Journal of Investigative Medicine*. 45(2). 1997. 99-108.
- [27] Einstein AJ. Wu HS. Sanchez M. and Gil J. Fractal characterisation of chromatin appearance for diagnosis in breast cytology. *Journal of Pathology*. 185(4):366-381, 1998 Aug.
- [28] Erler BS. Vitagliano P. and Lee S. Superiority of neural networks over discriminant functions for thalassemia minor screening of red blood cell microcytosis. *Archives of Pathology & Laboratory Medicine*. 119(4):350-354, 1995
- [29] Cesar, R.M., Jr. and Jelinek, H.F. (2002) Segmentation of retinal fundus vasculature in non-mydriatic camera images using wavelets. In: *Angiography Imaging: State-of-the-Art Acquisition, Image Processing and Applications Using Magnetic Resonance, Computer Tomography, Ultrasound and X-rays*. Eds. Suri, J. and Laxminarayan. T., Chapter 9. Academic Press, N.Y. (in print)
- [30] Michalski B., Mazurek U., Olejek A., Graniczka M., Loch T., Poreba R. and Wilczok T. Quantitative RT-PCR assay for mRNA of VEGF and histone H4 in the determination of proliferative and angiogenic activity in vulvar pathology. *Folia Histochemica et Cytobiologica* 39(Suppl. 2). 2001. 108-109.
- [31] Witten, I.H. and Frank, E.: *Data Mining: Practical Machine Learning Tools and Techniques with Java Implementations*. Morgan Kaufmann (1999).
- [32] R. Kohavi, The Power of Decision Tables, in: *Proceedings of the European Conference on Machine Learning, Lecture Notes in Artificial Intelligence 914* (Springer Verlag 1995) 174-189.
- [33] Fisher, R.A., 1936, The use of multiple measurements in taxonomic problems. *Annual Eugenics* 7 (part II):179-188. Reprinted in *Contributions to Mathematical statistics*, 1950, Wiley.
- [34] Quinlan, J.R., 1986, Induction of Decision Trees. *Machine Learning*, 1(1):81-106.
- [35] B.W. Silverman, *Density Estimation for Statistics and Data Analysis*, (Chapman and Hall, London, 1986).
- [36] Bayes. T., 1763, An essay towards solving a problem in the doctrine of chances. *Philosophical Transactions of the Royal Society of London* 53:370-418.
- [37] Albus, J. S. (1975). A New Approach to Manipulator Control: the Cerebellar Model Articulation Controller (CMAC). *Trans. ASME, Series G. Journal of Dynamic Systems, Measurement and Control*. 97, 220-233.
- [38] Cornforth, D. and Newth, D. (2001). The Kernel Addition Training Algorithm: Faster Training for CMAC Based Neural Networks. *Proc. Conf. Artificial Neural Networks and Expert Systems*, Otago.
- [39] Andjelkovic, A. V., Spencer, D. D. and Pachter, J. S. (1999) Visualization of Chemokine Binding Sites on Human Brain Microvessels. [Article] *Journal of Cell Biology*. 145(2):403-412.
- [40] B. Efron, Estimating the error rate of a prediction rule: improvement on cross-validation, *Journal of the American Statistical Association*, 78 (382) (1983) 316-330.